Skeletal Radiology (2019) 48:503–516
https://doi.org/10.1007/s00256-018-3079-1

REVIEW ARTICLE

The current status of MRI in the pre-operative assessment of intramedullary conventional appendicular osteosarcoma

Asif Saifuddin[1] · Ban Sharif[1] · Craig Gerrand[2] · Jeremy Whelan[3]

Received: 27 July 2018 / Revised: 8 September 2018 / Accepted: 16 September 2018 / Published online: 4 October 2018

Abstract

Osteosarcoma is the commonest primary malignant bone tumour in children and adolescents, the majority of cases being conventional intra-medullary high-grade tumours affecting the appendicular skeleton. Treatment is typically with a combination of neo-adjuvant chemotherapy, tumour resection with limb reconstruction and post-operative chemotherapy. The current article reviews the role of magnetic resonance imaging (MRI) in the pre-operative assessment of high-grade central conventional osteosarcoma.

Keywords Osteosarcoma · Magnetic resonance imaging · Magnetic resonance imaging in pre-operative assessment of osteosarcoma · Magnetic resonance imaging in local staging of osteosarcoma

Introduction

Osteosarcoma (OS) is the commonest primary malignant bone tumour in children, with an overall prevalence of 2–3/million/year, which increases to 8–11/million/year in the 15–19 age range [1–6], and accounts for over 10% of all solid cancers in adolescence (age 15–19 years) [7]. Although myeloma is the commonest primary bone tumour in adults, OS also shows a second peak in adults in the 7th–8th decades [7]. OS is classified according to the World Health Organisation (WHO) classification [8], with conventional high-grade central OS (HG-OS) being the commonest sub-type accounting for 75–80% of all cases [4, 6]. These tumours may show a mixed histological pattern or be predominantly osteoblastic, chondroblastic or fibroblastic [9]. Other histological variants include telangiectatic [10], small cell [11] and giant cell (osteoclast)-rich [12].

Due to the rarity of these tumours, management within specialist centres is mandatory [3, 7]. The aims of treatment are to achieve long-term disease-free survival with acceptable physical function, and this is currently achieved for the majority of patients by a combination of pre-and post-operative chemotherapy together with resection of the tumour and reconstruction with an endoprosthetic replacement (EPR) [13, 14]. Primary amputation is required in approximately 5–10% of cases, while limb reconstruction in the very young is achieved by a variety of techniques [15]. Imaging plays a vital role in the management of HG-OS, including lesion characterisation, local and distant staging, biopsy guidance and evaluation of response to neo-adjuvant chemotherapy [16–18]. The aim of this article is to review the current status of magnetic resonance imaging (MRI) in the pre-operative assessment of HG-OS involving the appendicular skeleton.

Lesion characterisation

HG-OS typically involves the metaphyses of major long bones, the distal femur, proximal tibia and proximal humerus being the commonest sites. Primary diaphyseal HG-OS is also recognised, tending to present in an older age group, having a greater tumour extent than metaphyseal HG-OS, and a greater risk of pathological fracture [19, 20].

Radiographic assessment is still mandatory in the initial assessment of HG-OS. The classical radiographic features of

✉ Ban Sharif
ban.sharif@nhs.net

[1] Department of Imaging, Royal National Orthopaedic Hospital, Brockley Hill, Stanmore HA7 4LP, UK

[2] Department of Orthopaedic Oncology, Royal National Orthopaedic Hospital, Brockley Hill, Stanmore HA7 4LP, UK

[3] Medical Oncology, University College London Hospital, 235 Euston Rd, London NW1 2BU, UK

aggressive lytic bone destruction, osteoblastic matrix, extra-osseous extension, Codman's triangle and periosteal reaction allow a confident radiological diagnosis in the majority of cases (Fig. 1a) [21]. Alternatively, the lesion may be purely osteoblastic (Fig. 1b) or lytic (Fig. 1c), in which case the age at presentation and classical metaphyseal location are still suggestive. However, in purely lytic lesions, MRI may be of additional value in lesion characterisation.

In a recent study of telangiectatic OS [10], only four of 26 cases (15.4%) showed radiographic matrix mineralisation. However, the aggressive growth pattern with cortical destruction and soft tissue mass helped in the radiographic differentiation from aneurysmal bone cyst (ABC). MRI demonstrated multiple large (72.7%) or small (26.3%) cystic spaces, fluid-fluid levels (63.6%), soft tissue mass (100%) (Fig. 2), and thick peripheral and septal enhancement (100%). A misdiagnosis of ABC was made on biopsy in 34.6% of cases.

Giant cell (osteoclast) rich OS (GCR-OS) is also a predominantly osteolytic lesion, occurring most commonly in the proximal tibia [12]. The mean age of 26 years and predominantly eccentric meta-epiphyseal location may mimic giant cell tumour (GCT) of bone. MRI shows no distinctive features, but the presence of a large extra-osseous mass may be more suggestive of GCR-OS than GCT.

The MRI features of chondroblastic OS have also been described and compared with other types of OS and chondrosarcoma. Chondroblastic OS may uncommonly show lobular hyperintensity (Fig. 3a) and a septal/nodular/peripheral rim enhancement pattern similar to chondrosarcoma (Fig. 3b) [22]. Also, the use of diffusion-weighted imaging (DWI) may allow differentiation of chondroblastic OS from other types of OS and from chondrosarcoma [23, 24].

The clinical and imaging features of primary diaphyseal OS have been compared to metaphyseal OS. Diaphyseal OS accounts for just under 4% of all long bone OS [20]. It has a more lytic appearance on radiographs and a much larger soft tissue mass [19]. In patients with lytic diaphyseal OS, MRI may help characterisation by demonstrating the large soft tissue mass. However, the finding of a lytic diaphyseal lesion with a large soft tissue mass would also be consistent with Ewing sarcoma (ES), although ES tends to occur in a younger age group.

Local staging

Accurate local staging of OS is required to plan surgical resection. Local staging may be subdivided into intra-osseous and extra-osseous tumour extent [16]. Intra-osseous tumour extent determines the level of bone resection, and must include any identified skip metastases. Skip metastases represent focal areas of intra-osseous tumour which are separated from the main tumour by normal marrow. In addition, it may demonstrate the possibility of joint sparing surgery in the immature skeleton when metaphyseal tumour has not extended to involve the growth plate [25]. Extra-osseous staging determines the potential for limb salvage surgery based on the relationship of tumour to the neurovascular structures and the degree of muscle involvement, while demonstration of extension into the joint will require extra-articular resection [14, 26].

Intra-osseous staging

A non-contrast T1-weighted spin echo (T1W SE) sequence remains the gold standard for determination of intra-osseous tumour extent, due to the high contrast between intermediate-to-low SI tumour and hyperintense medullary fatty marrow (Fig. 2b) [27]. Several recent studies have demonstrated that longitudinal tumour extent on T1W SE images compares most favourably with tumour length measured on resection specimens. Jin et al. [28] demonstrated that median tumour length on resection specimens was approximately 4 mm greater than on T1W MRI. In 255 patients with primary malignant tumours of the long bone (223 with appendicular OS), MRI demonstrated tumour length accurately in 10.6%, overestimated tumour length in 31% and underestimated tumour length in 58.4% of cases. The maximal difference between resection specimen tumour length and MRI assessment was 18 mm. Similarly, Thompson et al. [29] investigated the relationship between T1

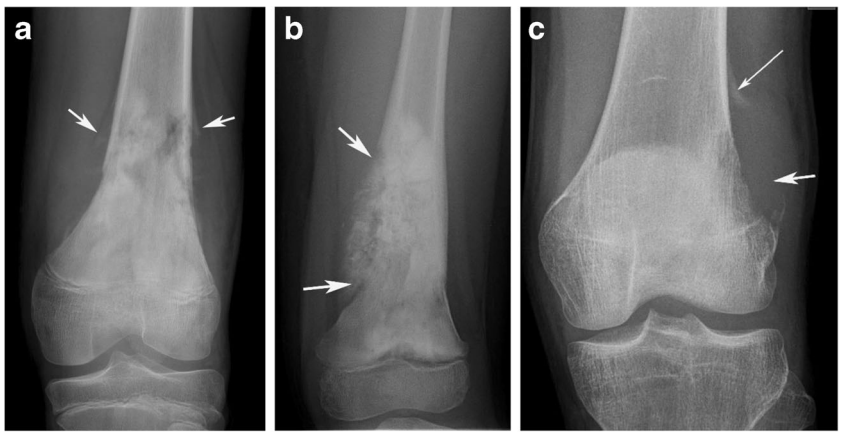

Fig. 1 Radiographic appearances of high-grade osteosarcoma (HG-OS). **a** AP radiograph of the distal femur showing aggressive mixed lytic and sclerotic bone destruction with a Codman's triangle (*arrows*). **b** AP radiograph of the distal femur showing an extensive osteoblastic distal femoral lesion (*arrows*). **c** AP radiograph of the distal femur showing purely lytic bone destruction (*arrow*) and a Codman's triangle (*thin arrow*)

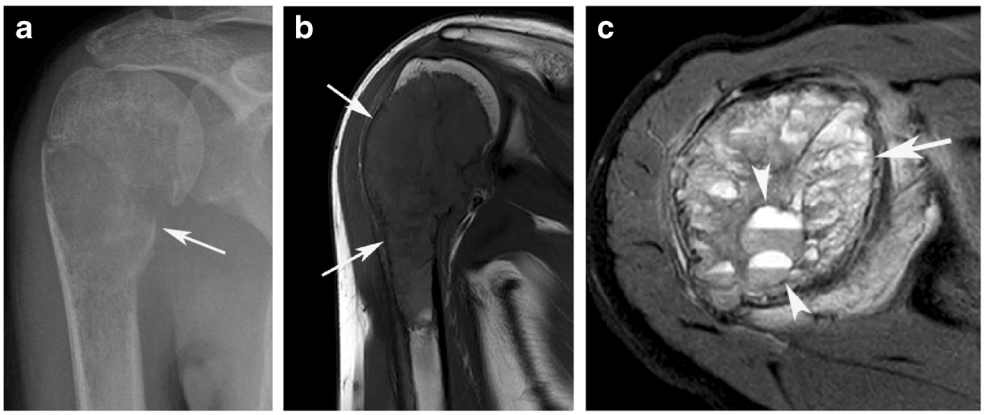

Fig. 2 Telangiectatic OS. **a** AP radiograph of the right shoulder showing a purely lytic proximal humeral tumour (*arrow*). **b** Coronal T1-weighted turbo spin echo (T1W TSE) MR image showing an intermediate signal intensity (SI) lesion (*arrows*). **c** Axial fat-suppressed proton density weighted fast spin-echo (PDW FSE) MR image showing multiple cystic spaces (*arrow*) and fluid-fluid levels (*arrowheads*)

and T2W images obtained before and after neo-adjuvant chemotherapy with tumour extent from resection specimens, and found that T1W SE images obtained following neo-adjuvant chemotherapy had the strongest correlation with resection specimens (Fig. 4). The mean difference between MRI and histopathological margins was 5.9 mm (SD = 4.5 mm). Conversely, the use of T2W SE, short-tau inversion recovery (STIR) and post-contrast fat-suppressed T1W SE sequences has been shown to overestimate intra-osseous tumour extent [30]. The reported difference in the measurements between MRI and resection specimens could in part be due to technical factors, MRI demonstrating the intra-osseous tumour length on multiple sagittal and/or coronal images through the whole extent of the bone, whereas the resected specimen may be sectioned only once or twice in the coronal or sagittal plane at pathological assessment.

The accurate assessment of intra-osseous tumour extent may become difficult in the presence of abundant red marrow, as can be found in very young patients or following neoadjuvant chemotherapy. In the latter situation, Deng et al. [31] demonstrated the development of marrow signal abnormality on post-chemotherapy T1W SE MRI in approximately 60% of patients with appendicular OS. This was classified as either 'continuous diffuse', 'discontinuous diffuse' (Fig. 4a) or 'discontinuous island-like' (Fig. 5a) in its relationship to the tumour and its morphology. The marrow lesion had SI that was hypointense to medullary fatty marrow but hyperintense to skeletal muscle, and histological assessment of these areas on resection specimens showed hyperplastic red marrow. In cases where both limbs were imaged, the findings were bilateral and symmetrical (Fig. 5b) and were considered to be due to the use of granulocyte colony stimulating factor (GCSF), which is routinely used to treat neutropenia during chemotherapy. When hyperplastic red marrow is continuous with the tumour, the tumour margin may be difficult to determine accurately based on T1W SE images. In this situation, the use of chemical shift imaging (CSI) may aid differentiation between tumour and red marrow. CSI is based on the principle that protons attached to fat and water precess with slightly different frequencies. This property allows differentiation between voxels containing both fat and water, such as in the setting of marrow hyperplasia or marrow oedema, and voxels that contain no fat due to complete replacement of the marrow by tumour tissue. In the former situation, there will be a greater than 20% reduction of signal between in-phase (IP) and opposed-phase (OP) gradient echo images, while in the latter the drop in signal between IP and OP images will be less than 20% [32]. Del Grande et al. [33] compared CSI with T1W SE images in 17 patients with appendicular bone tumours and showed a very good correlation between the two (Figs. 6a and b), with a mean difference in measurements of only 1.7 mm (range, 0–13.2 mm). Due to the relative lack of red

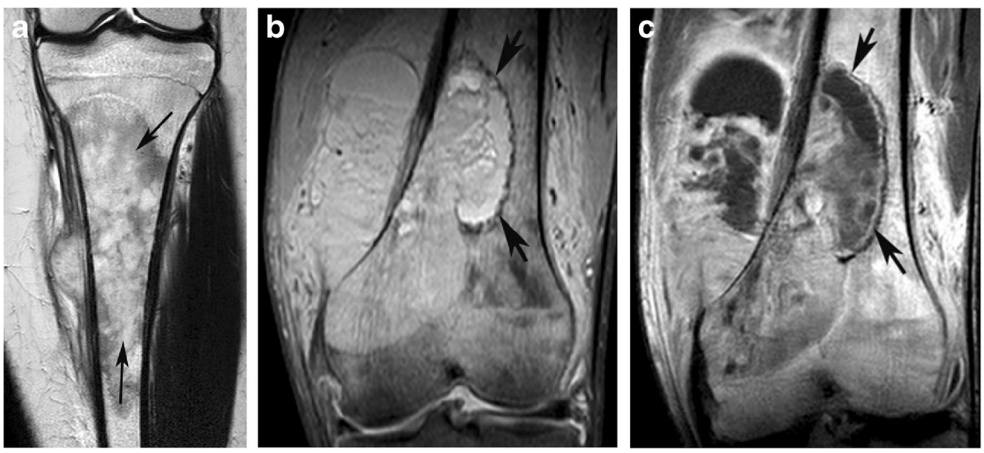

Fig. 3 Chondroblastic OS. **a** Coronal T2-weighted fast spin-echo (T2W FSE) MR image of the femur showing a lobular hyperintense morphology to the tumour (*arrows*). **b** Coronal short tau inversion recovery (STIR) and **c** post-contrast T1W SE MR images demonstrating rim enhancement of a portion of the lobular hyperintense intramedullary component of the lesion (*arrows*)

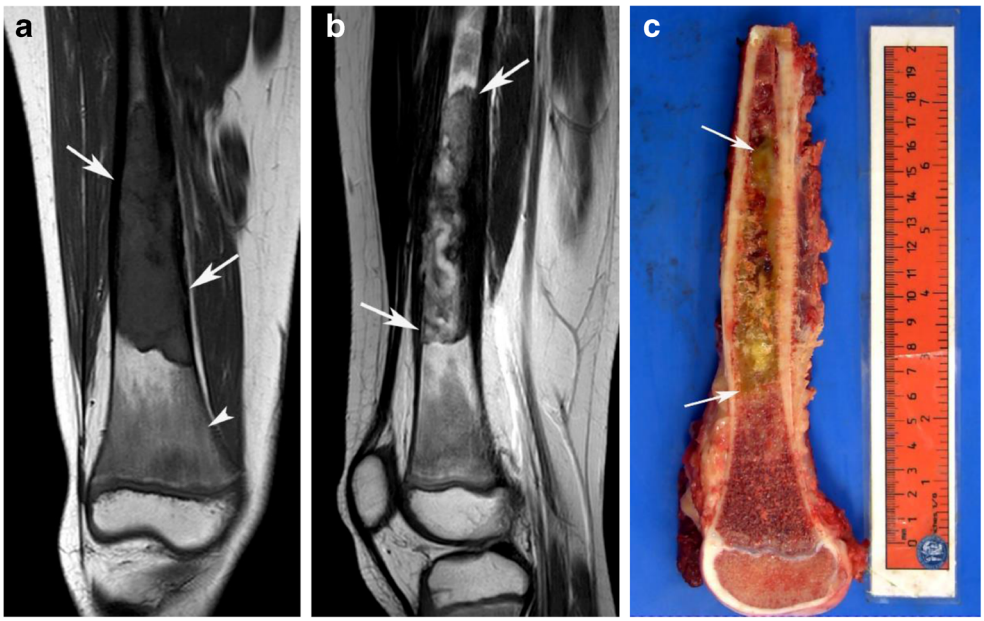

Fig. 4 Post-chemotherapy intramedullary staging. **a** Coronal T1W TSE MR image of the distal femur showing intermediate SI tumour (*arrows*) contrasting against hyperintense medullary fat. Hyperplastic red marrow is present in the distal metaphysis (*arrowhead*) due to granulocyte colony stimulating factor (GCSF) effect. **b** Sagittal T2W FSE MR image and **c** sagittal resection specimen show the tumour (*arrows*), which was measured at 10.5 cm in the mid-sagittal plane on MRI and on the resection specimen

marrow in the appendicular skeleton, they found no benefit of CSI compared to T1W SE images. However, for axial lesions where red marrow was more abundant, CSI was able to demonstrate tumour infiltration when the appearances were equivocal on T1W. Similarly, the presence of marrow hyperplasia could make skip metastases less conspicuous, in which case CSI may be of value (Figs. 6c and d).

Skip metastases

Skip metastases occur most commonly within the same bone (Fig. 7a) or rarely in the adjacent bone, when they are referred to as trans-articular skip metastases (Fig. 7b) [34]. They can be identified by MRI, appearing as single or multifocal (Fig. 7c) areas of marrow abnormality with similar signal characteristics to the original tumour. The reported prevalence of skip metastases in long bone osteosarcoma varies from 1.4% [35] to 6.5% [36], and MR imaging of the whole bone with at least a coronal T1W SE sequence is required to identify these, particularly since they may be occult on radiography and bone scintigraphy [35, 37]. However, the sensitivity and specificity of whole bone MRI has not been established with regards the diagnosis of skip lesions. A study by Sajadi et al. [36] described 10 skip metastases of which only eight were identified on pre-operative whole-bone MRI. Similarly, Kager et al. [35] reported on 24 patients with unequivocally proven skip metastases. Of these, 15 skip metastases were identified in 18 patients who had pre-operative MRI. Therefore, it is clear that skip metastases may

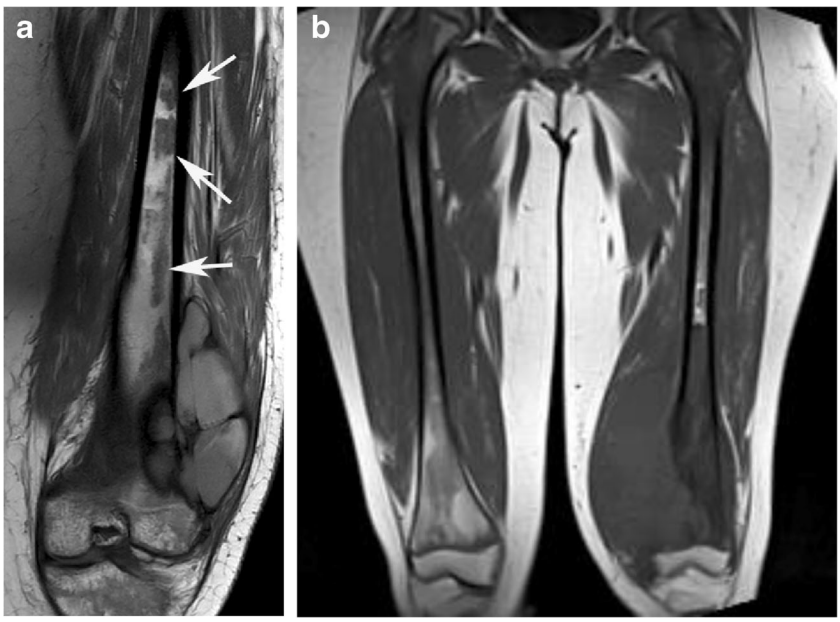

Fig. 5 Post-chemotherapy marrow changes. **a** Coronal T1W TSE MR image showing a distal femoral HG-OS and multiple 'island-like' areas of marrow hyperplasia (*arrows*). **b** Coronal T1W SE MR image of both femora showing a left distal femoral HG-OS with bilateral, symmetrical marrow changes due to GCSF

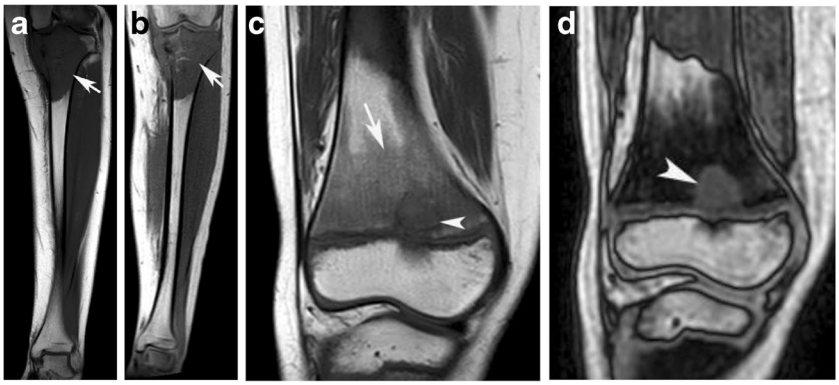

Fig. 6 Chemical shift imaging. **a** Coronal T1W TSE MR image of the tibia showing the intra-medullary tumour extent (*arrow*). **b** Corresponding in-phase coronal CSI showing good correlation of intra-medullary tumour extent (*arrow*). **c** Coronal T1W TSE MR image of the distal femur showing hyperplastic red marrow (*arrow*) which is partially obscuring a skip metastasis (*arrowhead*). **d** Opposed-phase coronal CSI more clearly demonstrates the skip lesion (*arrowhead*) within the hypointense red marrow

be occult on MRI. Also, the possibility that an intra-osseous lesion which has MRI features of a skip metastasis representing an alternative pathology such as focal marrow hyperplasia (Fig. 7d) or a small enchondroma has to be considered, since it is known that incidental enchondromas can be identified in 2.9% of knee MRI studies [38] and 2.1% of shoulder MRI studies [39]. In such cases, a more detailed MRI study of the lesion, possibly with the addition of CT to look for classical matrix mineralisation could be undertaken to allow a confident diagnosis without the need for biopsy. However, in a situation where a potential skip metastasis is located well away from the main tumour and its resection would require a change in surgical technique, biopsy of the lesion may be necessary to obtain histological confirmation of its nature.

The relevance of skip metastases has also been discussed. Failure of resection of a skip lesion is a cause of local recurrence [40]. Also, several studies have indicated that patients with skip metastases at presentation have a significantly higher risk of local recurrence, distant metastases and a worse survival, and should therefore be considered as having stage 3 disease [36, 41]. Conversely, Kager et al. [35] reported 50% disease-free survival at a mean of 4.4 years in patients with skip metastases, the location of the skip metastasis in the same bone and a good response to chemotherapy being favourable factors.

Extra-osseous staging

The vast majority of long bone intra-medullary HG-OS have extended through the bone cortex at the time of presentation, equating to at least stage 2B of the Enneking staging system [42]. HG-OS commonly initially extends out of the cortex before elevating and stretching the periosteum. The tumour may not be confined by the elevated periosteum, suggesting biologic aggressiveness, and the location of such extra-periosteal extension should be specifically described. The relationship of extra-osseous tumour to the major neurovascular structures and extent

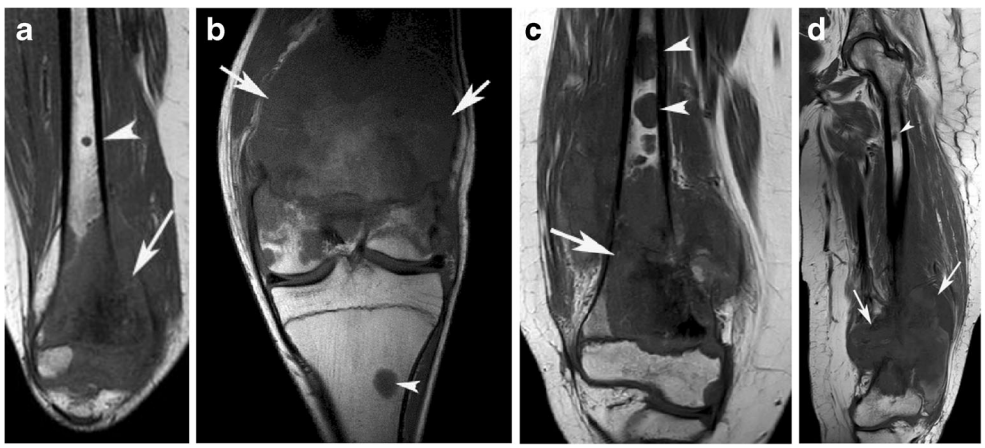

Fig. 7 Skip metastases. **a** Coronal T1W TSE MR image showing a distal femoral HG-OS (*arrow*) and a proximal skip metastasis (*arrowhead*). **b** Coronal T1W SE MR image showing a distal femoral HG-OS (*arrows*) and a trans-articular skip metastasis in the proximal tibia (*arrowhead*). **c** Coronal T1W TSE MR image showing a distal femoral HG-OS (*arrow*) and multiple proximal skip metastases (*arrowheads*). **d** False positive 'skip' lesion. Coronal T1W SE MR image showing a distal femoral OS (*arrows*) with a small proximal femoral lesion (*arrowhead*) diagnosed on MRI as a skip metastasis, but confirmed at histology to represent focal marrow hyperplasia

of involvement of muscle compartments are significant determinants for the ability to perform limb salvage procedures. The identification of a fat plane between tumour and neurovascular structures is an important feature to identify, and therefore non-fat-suppressed sequences should be used to assess this. A small number of studies have assessed the ability of MRI to identify the relationship of extra-osseous tumour to the neurovascular bundle (NVB). Van Trommel et al. [43] reviewed MRI and surgical findings in 32 distal femoral HG-OS, and found that if no tumour was seen involving the neurovascular structures, this was always the case at surgery (Fig. 8a). When MRI showed a close relationship between tumour and nerve (Fig. 8b), a safe surgical plane could be achieved in 73% cases, and similarly in 46% of cases when there was possible vascular involvement. Whenever there was definite tumour involvement of neurovascular structures, this was almost invariably correct at pathological exanimation (Fig. 8c). Putta et al. [30] defined involvement to be present if the NVB was either completely surrounded by tumour or when at least 50% was surrounded with loss of the fat plane on at least one axial section, using a combination of T2W and fat-suppressed post-contrast T1W sequences. They diagnosed NVB involvement in 3 of 21 (14%) patients with aggressive bone tumours (16 HG-OS). At surgery, only one patient had NVB involvement, resulting in sensitivity, specificity, PPV and NPV of 100, 90, 33.3, and 100%, respectively. Similarly, Wu et al. [44] reported sensitivity, specificity, PPV and NPV of 50, 100, 100, and 94%, respectively in 34 patients with HG-OS, but did not define their criteria for NVB involvement. Jeon et al. [45] correlated relationship of tumour to NVB on pre-operative MRI with local recurrence (LR) in patients who had a poor response to chemotherapy. An adequate margin with regards the NVB was defined as a clear fat plane between tumour and the NVB, while an inadequate margin was defined as tumour abutting the NVB or encasement of the NVB. The finding of tumour abutting the NVB on pre-operative MRI in poor responders who underwent limb salvage was associated with a high incidence of LR in the peri-neurovascular soft tissues. Masrouha et al. correlated non-mass-like abnormal signal intensity adjacent to the extra-osseous component of the tumour with pathological findings in 27 patients with HG-OS [46]. These abnormal signal areas were classified as being either bulky (> 1 cm thick) (Fig. 9a), feathery (Fig. 9b) or having linear (< 1 cm thick) fluid SI (Fig. 9c). The bulky appearance was seen in seven cases, four of which demonstrated viable tumour in the resection specimens, whereas the feathery appearance was never associated with viable tumour. In 1 of 11 cases, the linear appearance was associated with viable tumour. Oedematous changes in the surrounding soft tissues are referred to as the reactive zone.

The relationship of extra-osseous tumour to the NVB will be altered by neo-adjuvant chemotherapy. In a study looking at the effects of neo-adjuvant chemotherapy on operative planning in distal femoral HG-OS, Jones et al. showed that involvement of the NVB by both oedema and tumour could either decrease (Fig. 10a and b) or increase (Figs. 10c and d) when comparing MRI studies at initial diagnosis with post-chemotherapy MRI [47].

Joint involvement

The presence of joint involvement requires extra-articular resection and reconstruction [14, 26]. However, there does not seem to be a consensus on what constitutes joint involvement. The demonstration of tumour tissue within the synovial space and pathological fracture into the joint are considered unequivocal evidence of joint involvement. However, it is unclear if involvement of peri-articular structures such as the tendons and ligaments necessitates extra-articular resection (Fig. 11a). A pathological study of joint invasion by primary metaphyseal sarcomas demonstrated invasion of articular cartilage in one-third of cases, while in over 50% of cases tumour extended under the capsular insertion to involve the margin of the articular cartilage, leaving only a pseudo-capsule between the tumour and joint. Involvement of the osseous-tendinous junction of the cruciate ligaments with extension into the knee was also commonly identified [48]. Similarly, a pathological study of 27 cases of HG-OS near joints showed that there was never complete penetration of tumour through the articular cartilage, although peripheral extension of tumour around

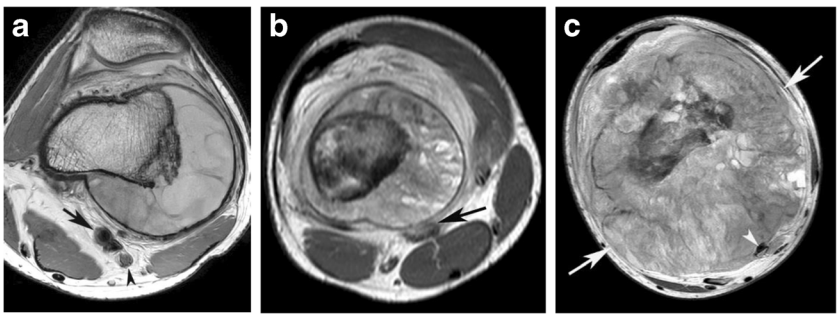

Fig. 8 Extra-osseous staging. **a** Axial PDW FSE MR image through the distal femur showing a clear fat plane between the extra-osseous tumour and the popliteal vessels (*arrow*) and tibial nerve (*arrowhead*). **b** Axial PDW FSE MR image through the femur showing the extra-osseous tumour contacting the femoral vessels (*arrow*). **c** Axial PDW FSE MR image through the distal femur showing a circumferential extra-osseous tumour mass (*arrows*) encasing the popliteal artery (*arrowhead*)

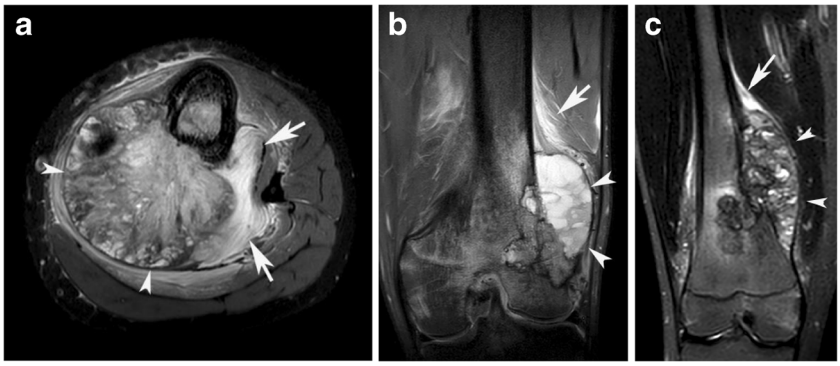

Fig. 9 Non-mass like soft tissue changes adjacent to tumour. **a** Axial fat-suppressed PDW FSE MR image showing bulky signal abnormality (*arrows*) adjacent to a proximal tibial HG-OS (*arrowheads*). **b** and **c** Coronal STIR MR images showing feathery (arrow-b) and linear fluid (arrow-c) signal changes adjacent to the extra-osseous component of HG-OS of the distal femur (*arrowheads*)

the joint margin was seen in more than one-third of cases. The authors also found that if pre-operative MRI showed no definite evidence of joint involvement, then this was never identified pathologically allowing safe intra-articular resection to be undertaken. In two cases, intra-articular extension was assumed based on MRI showing extension of tumour into the cruciate ligaments with subsequent extra-articular resection. However, in both cases no tumour was seen in the joint on review of the resection specimen [49]. Trans-articular spread of tumour into adjacent joints via other normal anatomical structures such as the ligamentum teres in the hip [50] and the synovium of the knee joint [51] has also been rarely described with high-grade malignant bone tumours, and should be assessed for in cases of HG-OS. However, this is most frequently reported in the sacroiliac joints [52].

Few studies have assessed the accuracy of MRI with regards joint involvement by HG-OS. Schima et al. [53] considered joint involvement to be present if a contrast-enhancing mass was seen extending into the joint, either by disruption of the joint capsule or by extension through destroyed cortical bone and articular cartilage. Extension into the cruciate ligaments was also considered to represent involvement of the knee joint, even though they are extra-synovial structures. Pathological specimens revealed joint involvement in approximately 22% of cases. Using these criteria, MRI had a sensitivity of 100% but a specificity of only 69%, with an erroneous diagnosis of joint involvement being made in nearly one-quarter of cases. Similarly, Wu et al. [44] reported sensitivity and specificity of 100 and 60% respectively for joint involvement, but did not state precisely what criteria were used. Putta et al. [30] defined

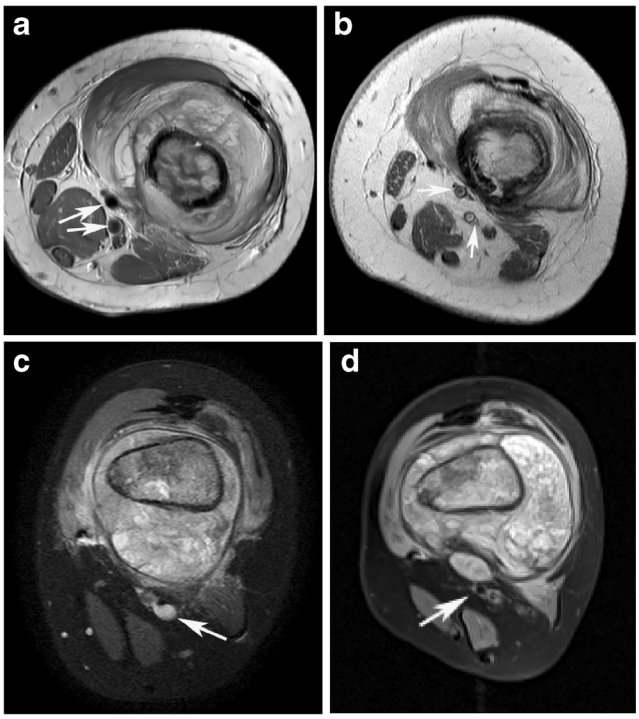

Fig. 10 Extra-osseous staging-effect of neo-adjuvant chemotherapy. **a** Pre-chemotherapy and **b** post-chemotherapy axial PDW FSE MR images in a patient with distal femoral HG-OS showing tumour originally abutting the NVB (arrows-a), with a clear plane between tumour and the NVB (arrows-b) following neo-adjuvant chemotherapy. The patient had a good response to chemotherapy. Extra-osseous staging-effect of neo-adjuvant chemotherapy. **c** Pre-chemotherapy and **d** post-chemotherapy axial fat-suppressed PDW FSE MR images in a patient with distal femoral HG-OS showing tumour originally separate from the NVB (arrow-a), with tumour abutting the NVB (arrow-b) following neo-adjuvant chemotherapy. The patient had a poor response to chemotherapy

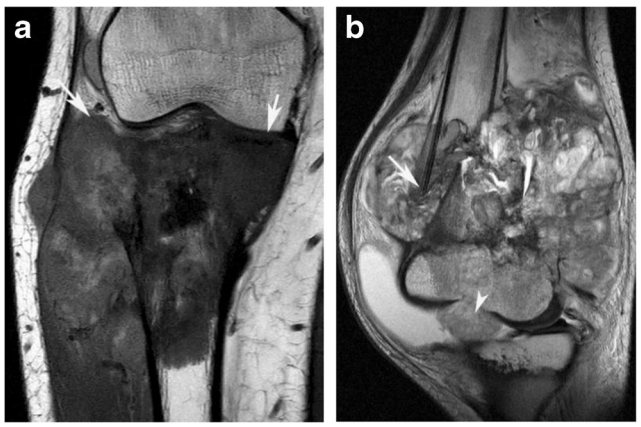

Fig. 11 Joint involvement. **a** Coronal T1W TSE MR image showing a proximal tibial HG-OS with extensive involvement of the sub-articular bone and lateral capsule (*arrows*). However, the patient was successfully treated with an intra-articular resection and proximal tibial EPR. **b** Sagittal T2W FSE MR image showing a large distal femoral HG-OS complicated by pathological fracture (*arrow*) and intra-articular extension (*arrowhead*)

joint involvement to be present if a mass was seen within the joint space (Fig. 11b), or if there was definite breach of articular cartilage by the tumour with or without a mass projecting into the joint cavity. Involvement of the cruciate ligaments was also taken as evidence of joint involvement. Based on these criteria, MRI diagnosed joint involvement in 28% of patients with sensitivity, specificity, PPV, and NPV being 100, 93, 83, and 100%, respectively when compared to pathological examination. Therefore, it seems clear that there is a tendency for MRI to overestimate joint involvement, which may result in a higher rate of extra-articular resection.

Distant staging

Metastatic disease in HG-OS is reported in 15–23% of cases at presentation, being commoner in older patients, those with an axial location of the primary tumour, those with greater tumour size, and those with a lower human development index (HDI) [54–56]. The lungs are the commonest site of metastases (86%) followed by the skeleton (24%) [57]. Therefore, distant staging is traditionally limited to assessment of the lungs with chest radiography and non-contrast chest CT, and the skeleton with 99^{m}-Tc whole body bone scintigraphy [7, 58].

An early study comparing whole body MRI (WB-MRI) with skeletal scintigraphy and FDG-PET for the detection of bone metastases in 39 children and young adults with a variety of malignant tumours showed FDG-PET to be the most sensitive technique, and WB-MRI to be more sensitive than scintigraphy. However, only three of the patients had HG-OS [59]. More recently, the superiority of [18] FDG-PET/CT compared to skeletal scintigraphy for identifying osseous metastases in HG-OS has been confirmed [60, 61]. Similarly, the superiority of WB-MRI and DWI compared to skeletal scintigraphy in the identification of skeletal metastases in a wide variety of paediatric and adult cancers has also been established [62–64], but there are no studies comparing WB-MRI with skeletal scintigraphy in a large cohort of patients with HG-OS.

Biopsy guidance

Confirmation of the diagnosis of HG-OS is essential prior to the commencement of neoadjuvant chemotherapy [2, 7]. Image-guided core needle biopsy is the technique of choice and has a high diagnostic accuracy [65, 66]. However, Interiano et al. [67] reported a significantly higher diagnostic accuracy for open biopsy compared to percutaneous biopsy in 104 patients with HS-OS, percutaneous biopsy being successful in only 73.1% of cases. Details of image guidance for percutaneous biopsies were not given.

The biopsy should be undertaken in a specialist centre by an experienced radiologist, the biopsy site having been discussed with the surgical oncologist to allow the needle track to be excised at the time of surgery. MRI can play an important role in planning the biopsy approach [68] demonstrating areas of haemorrhage/necrosis which can be avoided (Fig. 12a), and also allowing targeting of the extra-osseous component of the tumour (Fig. 12b) which can provide a high diagnostic yield [65]. Biopsy of a suspected skip metastasis located at a significant distance from the primary tumour may also be required, if this would lead to a major change in the surgical technique. Small skip metastases demonstrated by MRI may be occult on CT, and although CT guidance can be used to target such lesions based on comparison of anatomical landmarks, MR-guided needle biopsy is an alternative technique [69, 70].

Surgical staging systems

A variety of surgical staging systems are available for HG-OS, all of which involve assessment of local tumour extent and distant disease, as well as histological grade [2, 42]. Therefore, MRI plays a major role in surgical staging. The Enneking (Musculoskeletal Tumour Society-MSTS) system describes the local tumour extent as being either intra-compartmental or extra-compartmental, the vast majority of appendicular HG-OS being either Stage 2B (high-grade; extra-compartmental) (Fig. 13a) or less commonly Stage 3 (associated with regional or distant metastases). The American Joint Committee on Cancer (AJCC) staging system considers maximal tumour dimension as being the important local factor. Based on this system, most HG-OS are either stage 2A (high-grade; < 8 cm) (Fig. 13b) or stage 2B (high-grade; > 8 cm.) (Fig. 2b), and less commonly stage 3 (with skip metastases) (Figs. 7a, b and c), stage 4A (with pulmonary metastases) or stage 4B (with non-pulmonary metastases). However, these staging systems predict sarcoma-specific survival rather than local recurrence, which is strongly related to chemotherapy response and surgical margins. Jeys et al. [71] proposed a new surgical staging system for HG-OS which took into account these two factors and was more accurately able to predict

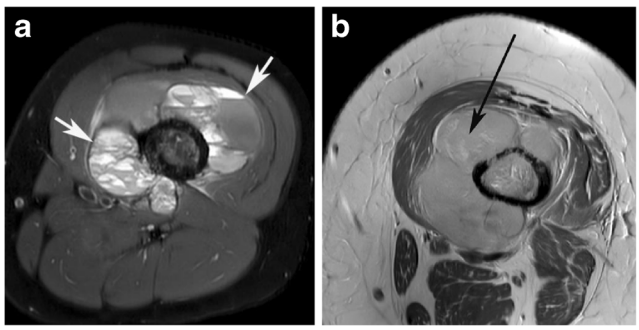

Fig. 12 Biopsy. **a** Axial fat-suppressed PDW FSE MR image showing a large extra-osseous mass demonstrating extensive blood-filled cystic spaces (*arrows*), which should be avoided for biopsy. **b** Axial PDW FSE MR image showing a large solid appearing extra-osseous mass which can be targeted for biopsy (*long black arrow*)

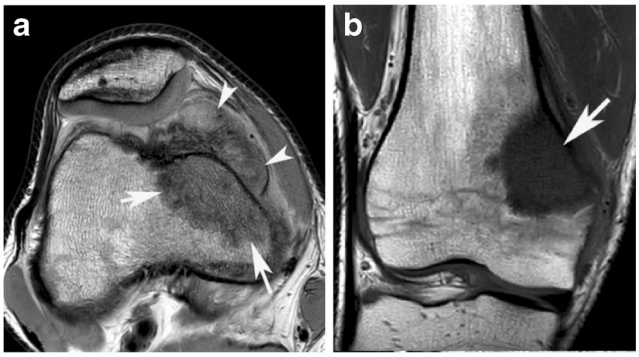

Fig. 13 Surgical staging. **a** Axial PDW FSE MR image showing a distal femoral HG-OS (*arrows*), with an anteromedial extra-osseous extension (*arrowheads*) consistent with stage 2B according to the MSTS staging system. **b** Coronal T1W TSE MR image showing a < 8 cm distal femoral HG-OS (*arrow*) consistent with stage 2A according to the AJCC staging system

5-year local recurrence-free survival than the MSTS margin classification, but pre-operative MRI features were not considered. More recently, a simplified staging system for sarcoma specific survival (the Vanderbilt system) has been proposed, which takes into account only histological grade and the presence of distant metastases to any site [72]. This system performs as well as the MSTS and AJCC staging systems for appendicular HG-OS.

Chemotherapy response and prognosis

The standard criterion for a good response to neo-adjuvant chemotherapy is the presence of greater than 90% necrosis in the resection specimen at detailed histopathological examination. Response of HG-OS to neoadjuvant chemotherapy has been extensively studied with a variety of MRI techniques. These include prediction of response at initial MRI based on tumour morphology, location and volume, and comparison of initial and post-chemotherapy studies using dynamic contrast enhanced MRI (DCE-MRI) and more recently DWI.

Prediction of response based on initial MRI

With regards tumour morphology, the presence of fluid-fluid level (FFLs) on initial MRI has been shown to correlate with poor chemotherapy response [73, 74]. In a study of 567 Enneking stage 2B HG-OS patients, 108 (19%) showed FFLs on initial MRI. These were typically lytic proximal humeral lesions that showed tumour enlargement following chemotherapy and poor histological response. In addition, those tumours showing FFLs involving < 1/3 of the tumour volume had a particularly poor response. Kim et al. assessed the relationship between tumour growth pattern on initial MRI with chemotherapy response, 5-year metastasis-free survival and overall survival in 347 patients with Enneking Stage 2B and AJCC stage 2 HG-OS. Tumour growth pattern was classified as concentric (64.8%) (Fig. 14a and b), eccentric (20.5%) (Fig. 13) and longitudinal (14.7%) (Fig. 14c). Eccentric tumours tended to be small and responded well to chemotherapy, while concentric tumours were large and responded poorly. In AJCC Stage 2B patients, longitudinal tumours were associated with a significantly better survival than concentric tumours [75].

Tumour size at presentation is also related to outcome. A variety of methods have been described to 'normalise' tumour volume to account for overall patient size and size of the bone of origin. Lee et al. [76] compared absolute and relative tumour size (the latter obtained by dividing absolute size by body surface area) with metastasis-free survival (MFS). In addition to poor histological response, large relative tumour plane (RTP), large relative tumour area (RTA) and large absolute tumour width (ATW) were associated with shorter MFS. Conversely, optimal survival was associated with a combination of good histological response and small RTP. Tumour axial ratio (TAR) [77] is a new technique calculated by dividing the maximal tumour dimension on axial MR images with a reference bone axial size (RBS) for tumours arising in the distal femur, proximal tibia, proximal humerus and proximal femur. When comparing TAR at initial presentation with TAR following neoadjuvant chemotherapy, a significant reduction in TAR was only identified in patients who survived for 5 years and those who were free of metastases. Large initial tumour volume and tumour growth after neoadjuvant chemotherapy are also poor prognostic factors [74].

Changes in tumour SI characteristics and tumour volume between initial staging MRI and post-chemotherapy MRI have also been compared to histological response. In an early study, Holscher et al. [78] identified that decreased tumour volume and reduction of T2-weighted SI in the extra-osseous component of the tumour correlated with good chemotherapy response. In a follow-up study, the same authors showed that an increase in tumour volume and increased or unchanged peri-tumoural oedema were associated with a poor response, whereas a reduced or unchanged tumour volume and decreased oedema were not predictive of a good response [79]. Increased tumour volume and increased T2-weighted SI of the extra-osseous component are also predictors of poor response after a single cycle of chemotherapy [80]. Shin et al. [81] calculated tumour volume on three dimensional MRI, and showed a significant relationship between changes in absolute and relative tumour volumes, as well as extra-osseous volume and chemotherapy response. Reduced or stable tumour volume was associated with good response with a sensitivity of 85%, specificity of 76% and PPV of 88%. However, other small studies have not shown a correlation between tumour volume changes and histological response [82, 83].

DCE-MRI

Chemotherapy induced changes in tumour neovascularity can be assessed with DCE-MRI using a variety of complex

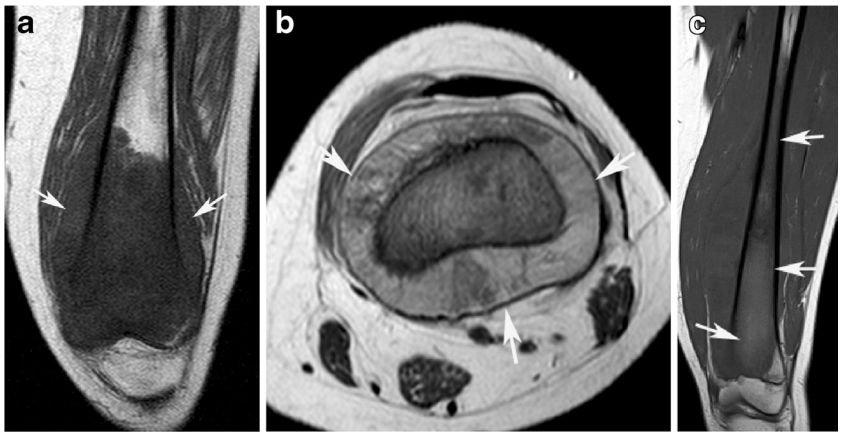

Fig. 14 Tumour growth patterns. **a** Coronal T1W SE and **b** axial PDW FSE MR images showing concentric growth of a distal femoral HG-OS (*arrows*). **c** Coronal T1W TSE MR image showing longitudinal growth of a femoral HG-OS (*arrows*)

parameters [82, 84–87]. Of these techniques, percentage slope analysis seems to be the simplest. A meta-analysis of six studies including 66 patients with HG-OS or Ewing sarcoma, defining good response as a greater than 60% reduction in the slope of the time intensity curve, demonstrated a pooled sensitivity and specificity of 73 and 83%, respectively, for DCE-MRI [88].

DWI

DWI is the latest MRI technique that has been used to assess chemotherapy response in HG-OS. DWI provides a measure of the mobility of water molecules within tissues. In theory, tumour tissue is expected to be highly cellular thus impeding the free movement of water, whereas necrotic tissue is acellular and allows free movement of water. This physical property can be quantified using the apparent diffusion coefficient (ADC), which may therefore be expected increase in the setting of adequate treatment response [89].

Multiple studies have demonstrated the ability of DWI to differentiate between good and poor treatment response in HG-OS. In an early study of eight paediatric limb HG-OS, Uhl et al. demonstrated significant changes in ADC values before and after chemotherapy, and also significantly increased ADC values in areas of necrotic tissue (mean 2.3 mm^2/s) compared to areas of viable tissue (mean 0.8 mm^2/s) following chemotherapy [90, 91]. Oka et al. investigated 22 patients with HG-OS, comparing average ADC and minimum ADC values pre- and post-chemotherapy, and found a significant increase in minimum ADC values in good responders (> 90% necrosis) compared to poor responders. However, the difference in average ADC values was not statistically significant [92]. Wang et al. performed DWI in 35 patients with appendicular HG-OS before and after neoadjuvant chemotherapy, showing a significant increase in ADC values overall following chemotherapy irrespective of the degree of response. Those patients with a good response showed significantly increased ADC values, and areas of necrotic tissue also showed significantly higher ADC values than areas of viable tissue [93]. Byun et al. compared PET-CT (difference in SUV), conventional MRI (difference in volume) and DWI (difference in ADC) in 28 patients with HG-OS before and after neoadjuvant chemotherapy. An increase in ADC value of 13% allowed prediction of good response with sensitivity, specificity and accuracy of 83, 73, and 78%, respectively. The specificity and accuracy increased to 87 and 85% respectively when DWI results were combined with PET-CT, but change in tumour volume was not predictive of response [94]. Wang et al. assessed chemotherapy response with DWI between different histological sub-types of HG-OS, identifying that tumour necrosis could be differentiated from viable tumour in fibroblastic and osteoblastic OS, but not in chondroblastic OS due to the inherently high ADC values of viable chondroblastic tissue [95]. Baunin et al. were able to use DWI to predict eventual chemotherapy response based on changes in ADC values between pre-chemotherapy and at mid-treatment [96]. A recent meta-analysis of five papers including a total of 106 patients has confirmed the ability of DWI to predict response to chemotherapy in HG-OS [97]. However, an important current limitation of DWI is the non-standardisation between MRI scanners and manufacturers. Also, variation of acquisition and analysis methods make ADC values non-comparable between different centres, and therefore invalidates the use of DWI in multicentre trials [98].

It is therefore clear that changes on MRI may reflect the response of HG-OS to chemotherapy, but the accuracy of this assessment may not be high enough to rely on when planning local surgical treatment. The accurate assessment of a tumour as having responded poorly to neoadjuvant chemotherapy may support primary amputation in some cases, rather than limb sparing surgery, particularly if the predicted anatomical margins will be close. In terms of systemic treatment, the benefit of changing chemotherapy agents on the basis of response has not been proven. Currently, the combination of methotrexate, doxorubicin and cisplatin (MAP) is typically used [99]. The addition of ifosfamide and etoposide (MAPIE) was the subject of the EURAMOS-1 study, and showed no survival advantage in patients showing a poor response to neoadjuvant chemotherapy [100].

Conclusions

MRI plays a vital role in the local staging of appendicular HG-OS, allowing accurate assessment of intra-osseous tumour extent based on which the level of bone resection can be safely planned. However, the sensitivity and specificity of MRI for the detection of skip metastases in a large group of patients has yet to be determined. The relationship of extra-osseous tumour to the major neurovascular structures allows determination of whether limb salvage surgery can be performed, but further studies are required to identify if MRI can predict the development of local recurrence based on the relationship of extra-osseous tumour to the NVB. The current literature would suggest that MRI overestimates joint involvement, which may result in an unnecessarily high rate of extra-articular resection. MRI has a limited role in tumour characterisation, but is of value in biopsy planning. A variety of techniques have demonstrated the ability of MRI to predict chemotherapy response, but the practical value of such information is presently limited due to a lack of chemotherapeutic options, although it may provide helpful information for surgical planning.

Compliance with ethical standards

Conflict of interest The authors declare that they have no conflict of interest.

References

1. Bielack S, Kempf-Bielack B, Von Kalle T, Schwarz R, Wirth T, Kager L, et al. Controversies in childhood osteosarcoma. Minerva Pediatr. 2013;65(2):125–48.
2. Kundu ZS. Classification, imaging, biopsy and staging of osteosarcoma. Indian J Orthop. 2014;48(3):238–46.
3. Biazzo A, De Paolis M. Multidisciplinary approach to osteosarcoma. Acta Orthop Belg. 2016;82(4):690–8.
4. Durfee RA, Mohammed M, Luu HH. Review of osteosarcoma and current management. Rheumatol Ther. 2016;3(2):221–43.
5. Taran S, Taran R, Malipatil N. Pediatric osteosarcoma: an updated review. Indian J Med Paediatr Oncol. 2017;38(1):33.
6. Misaghi A, Goldin A, Awad M, Kulidjian AA. Osteosarcoma: a comprehensive review. SICOT-J. 2018;4:12.
7. Gerrand C, Athanasou N, Brennan B, Grimer R, Judson I, Morland B, et al. UK guidelines for the management of bone sarcomas. Clin Sarcoma Res. 2016;6:7.
8. Fletcher CDM, Unni KK, Mertens F, Weltgesundheitsorganisation, International Agency for Research on Cancer, editors. Pathology and genetics of tumours of soft tissue and bone; [the WHO classification of tumours of soft tissue and bone presented in this book reflects the views of a working group that convened for an editorial and consensus conference in Lyon, France, April 24–28, 2002]. Lyon: IARC Press; 2002. 427 p. (World Health Organization Classification of tumours).
9. Klein MJ, Siegal GP. Osteosarcoma: anatomic and histologic variants. Am J Clin Pathol. 2006;125(4):555–81.
10. Gao Z-H, Yin J-Q, Liu D-W, Meng Q-F, Li J-P. Preoperative easily misdiagnosed telangiectatic osteosarcoma: clinical. Cancer Imaging. 2013;13(4):520–6.
11. Nakajima H, Sim FH, Bond JR, Unni KK. Small cell osteosarcoma of bone. Review of 72 cases. Cancer. 1997;79(11):2095–106.
12. Wang C-S, Yin Q-H, Liao J-S, Lou J-H, Ding X-Y, Zhu Y-B. Giant cell-rich osteosarcoma in long bones: clinical, radiological and pathological features. Radiol Med (Torino). 2013;118(8):1324–34.
13. Jeys LM, Kulkarni A, Grimer RJ, Carter SR, Tillman RM, Abudu A. Endoprosthetic reconstruction for the treatment of musculoskeletal tumors of the appendicular skeleton and pelvis. J Bone Jt Surg. 2008;90(6):1265–71.
14. Capanna R, Scoccianti G, Campanacci DA, Beltrami G, De Biase P. Surgical technique: extraarticular knee resection with prosthesis–proximal tibia-extensor apparatus allograft for tumors invading the knee. Clin Orthop Relat Res. 2011;469(10):2905–14.
15. Yao W, Cai Q, Wang J, Gao S. Treatment of osteosarcoma around the knee in skeletally immature patients. Oncol Lett [Internet]. 2017 [cited 2018 Jun 27]; Available from: http://www.spandidos-publications.com. https://doi.org/10.3892/ol.2017.6903
16. Saifuddin A. The accuracy of imaging in the local staging of appendicular osteosarcoma. Skelet Radiol. 2002;31(4):191–201.
17. Eftekhari F. Imaging Assessment of Osteosarcoma in Childhood and Adolescence: Diagnosis, Staging, and Evaluating Response to Chemotherapy. In: Jaffe N, Bruland OS, Bielack S, editors. Pediatric and Adolescent Osteosarcoma [Internet]. Boston, MA: Springer US; 2009 [cited 2018 Jun 27]. p. 33–62. Available from: http://link.springer.com/10.1007/978-1-4419-0284-9_3
18. Kaste SC. Imaging pediatric bone sarcomas. Radiol Clin N Am. 2011;49(4):749–65.
19. Wang C-S, Yin Q-H, Liao J-S, Lou J-H, Ding X-Y, Zhu Y-B, et al. Primary diaphyseal osteosarcoma in long bones: imaging features and tumor characteristics. Eur J Radiol. 2012;81(11):3397–403.
20. Iwata S, Nakamura T, Gaston CL, Carter SR, Tillman RM, Abudu A, et al. Diaphyseal osteosarcomas have distinct clinical features from metaphyseal osteosarcomas. Eur J Surg Oncol EJSO. 2014;40(9):1095–100.
21. Suresh S, Saifuddin A. Radiological appearances of appendicular osteosarcoma: a comprehensive pictorial review. Clin Radiol. 2007;62(4):314–23.
22. Yen C-H, Chang C-Y, Teng MM-H, Wu H-TH, Chen PC-H, Chiou H-J, et al. Different and identical features of chondroblastic osteosarcoma and chondrosarcoma: highlights on radiography and magnetic resonance imaging. J Chin Med Assoc. 2009;72(2):76–82.
23. Yakushiji T, Oka K, Sato H, Yorimitsu S, Fujimoto T, Yamashita Y, et al. Characterization of chondroblastic osteosarcoma: gadolinium-enhanced versus diffusion-weighted MR imaging. J Magn Reson Imaging. 2009;29(4):895–900.
24. Zeitoun R, Shokry AM, Ahmed Khaleel S, Mogahed SM. Osteosarcoma subtypes: magnetic resonance and quantitative diffusion-weighted imaging criteria. J Egypt Natl Cancer Inst. 2018;30(1):39–44.
25. Chen Y, Yu X, Xu S, Xu M, Song R. Impacts of tumor location, nature and bone destruction of extremity osteosarcoma on selection of limb salvage operative procedure: selection of limb salvage operation protocol for osteosarcoma. Orthop Surg. 2016;8(2):139–49.
26. Shahid M, Albergo N, Purvis T, Heron K, Gaston L, Carter S, et al. Management of sarcomas possibly involving the knee joint when to perform extra-articular resection of the knee joint and is it safe? Eur J Surg Oncol EJSO. 2017;43(1):175–80.
27. Shiga NT, Del Grande F, Lardo O, Fayad LM. Imaging of primary bone tumors: determination of tumor extent by non-contrast sequences. Pediatr Radiol. 2013;43(8):1017–23.
28. Jin T, Deng Z-P, Liu W-F, Xu H-R, Li Y, Niu X-H. Magnetic resonance imaging for the assessment of long bone tumors. Chin Med J. 2017;130(21):2547.

29. Thompson MJ, Shapton JC, Punt SE, Johnson CN, Conrad EU. MRI identification of the osseous extent of pediatric bone sarcomas. Clin Orthop. 2018;476(3):559–64.
30. Putta T, Gibikote S, Madhuri V, Walter N. Accuracy of various MRI sequences in determining the tumour margin in musculoskeletal tumours. Pol J Radiol. 2016;81:540–8.
31. Deng Z, Ding Y, Hao L, Zhang Q, Su Y, Niu X. Marrow signal mimicking tumor on MRI T1-weighted imaging after neoadjuvant chemotherapy in extremity osteosarcomas. J Bone Oncol. 2017;6:22–6.
32. Kohl CA, Chivers FS, Lorans R, Roberts CC, Kransdorf MJ. Accuracy of chemical shift MR imaging in diagnosing indeterminate bone marrow lesions in the pelvis: review of a single institution's experience. Skelet Radiol. 2014;43(8):1079–84.
33. Del Grande F, Tatizawa-Shiga N, Jalali Farahani S, Chalian M, Fayad LM. Chemical shift imaging: preliminary experience as an alternative sequence for defining the extent of a bone tumor. Quant Imaging Med Surg. 2014;4(3):173–80.
34. Enneking WF, Kagan A. "Skip" metastases in osteosarcoma. Cancer. 1975;36(6):2192–205.
35. Kager L, Zoubek A, Kastner U, Kempf-Bielack B, Potratz J, Kotz R, et al. Skip metastases in osteosarcoma: experience of the cooperative osteosarcoma study group. J Clin Oncol. 2006;24(10):1535–41.
36. Sajadi KR, Heck RK, Neel MD, Rao BN, Daw N, Rodriguez-Galindo C, et al. The incidence and prognosis of osteosarcoma skip metastases. Clin Orthop. 2004;426:92–6.
37. Bhagia SM, Grimer RJ, Davies AM, Mangham DC. Scintigraphically negative skip metastasis in osteosarcoma. Eur Radiol. 1997;7(9):1446–8.
38. Walden MJ, Murphey MD, Vidal JA. Incidental enchondromas of the knee. Am J Roentgenol. 2008;190(6):1611–5.
39. Hong ED, Carrino JA, Weber KL, Fayad LM. Prevalence of shoulder enchondromas on routine MR imaging. Clin Imaging. 2011;35(5):378–84.
40. Picci P, Sangiorgi L, Bahamonde L, Aluigi P, Bibiloni J, Zavatta M, et al. Risk factors for local recurrences after limb-salvage surgery for high-grade osteosarcoma of the extremities. Ann Oncol Off J Eur Soc Med Oncol. 1997;8(9):899–903.
41. Wuisman P, Enneking WF. Prognosis for patients who have osteosarcoma with skip metastasis. J Bone Joint Surg Am. 1990;72(1):60–8.
42. Jawad MU, Scully SP. In brief: classifications in brief: enneking classification: benign and malignant tumors of the musculoskeletal system. Clin Orthop. 2010;468(7):2000–2.
43. van Trommel MF, Kroon HM, Bloem JL, Hogendoorn PC, Taminiau AH. MR imaging-based strategies in limb salvage surgery for osteosarcoma of the distal femur. Skelet Radiol. 1997;26(11):636–41.
44. Wu HTH, Chang CY, Lin J, Chen TH, Chen WM, Wang SF. Preoperative MR imaging assessment of osteosarcoma: a radiological – surgical correlation. Chin J Radiol. 2001;26:9–16.
45. Jeon D-G, Song WS, Kong C-B, Cho WH, Cho SH, Lee JD, et al. Role of surgical margin on local recurrence in high-risk extremity osteosarcoma: a case-controlled study. Clin Orthop Surg. 2013;5(3):216.
46. Masrouha KZ, Musallam KM, Samra AB, Tawil A, Haidar R, Chakhachiro Z, et al. Correlation of non-mass-like abnormal MR signal intensity with pathological findings surrounding pediatric osteosarcoma and Ewing's sarcoma. Skelet Radiol. 2012;41(11):1453–61.
47. Jones KB, Ferguson PC, Lam B, Biau DJ, Hopyan S, Deheshi B, et al. Effects of neoadjuvant chemotherapy on image-directed planning of surgical resection for distal femoral osteosarcoma. J Bone Joint Surg Am. 2012;94(15):1399–405.
48. Simon MA, Hecht JD. Invasion of joints by primary bone sarcomas in adults. Cancer. 1982;50(8):1649–55.
49. Quan GMY, Slavin JL, Schlicht SM, Smith PJ, Powell GJ, Choong PFM. Osteosarcoma near joints: assessment and implications. J Surg Oncol. 2005;91(3):159–66.
50. Alkalay D, Kollender Y, Mozes M, Meller I. Transarticular tumor invasion via ligamentum teres. A clinical-pathologic study of 12 patients. Acta Orthop Scand. 1998;69(1):29–30.
51. Li X, Zhang Z, Latif M, Chen W, Cui J, Peng Z. Synovium as a widespread pathway to the adjacent joint in undifferentiated high-grade pleomorphic sarcoma of the tibia: a case report. Medicine (Baltimore). 2018;97(8):e9870.
52. Abdelwahab IF, Miller TT, Hermann G, Klein MJ, Kenan S, Lewis MM. Transarticular invasion of joints by bone tumors: hypothesis. Skelet Radiol. 1991;20(4):279–83.
53. Schima W, Amann G, Stiglbauer R, Windhager R, Kramer J, Nicolakis M, et al. Preoperative staging of osteosarcoma: efficacy of MR imaging in detecting joint involvement. AJR Am J Roentgenol. 1994;163(5):1171–5.
54. Kaste SC, Pratt CB, Cain AM, Jones-Wallace DJ, Rao BN. Metastases detected at the time of diagnosis of primary pediatric extremity osteosarcoma at diagnosis: imaging features. Cancer. 1999;86(8):1602–8.
55. Miller BJ, Cram P, Lynch CF, Buckwalter JA. Risk factors for metastatic disease at presentation with osteosarcoma: an analysis of the SEER database. J Bone Jt Surg-Am Vol. 2013;95(13):e89 1–8.
56. Marko TA, Diessner BJ, Spector LG. Prevalence of metastasis at diagnosis of osteosarcoma: an international comparison: prevalence of metastatic osteosarcoma at diagnosis. Pediatr Blood Cancer. 2016;63(6):1006–11.
57. Salah S, Ahmad R, Sultan I, Yaser S, Shehadeh A. Osteosarcoma with metastasis at initial diagnosis: current outcomes and prognostic factors in the context of a comprehensive cancer center. Mol Clin Oncol. 2014;2(5):811–6.
58. Roberts CC, Daffner RH, Weissman BN, Bancroft L, Bennett DL, Blebea JS, et al. ACR appropriateness Criteria® on metastatic bone disease. J Am Coll Radiol. 2010;7(6):400–9.
59. Daldrup-Link HE, Franzius C, Link TM, Laukamp D, Sciuk J, Jürgens H, et al. Whole-body MR imaging for detection of bone metastases in children and young adults: comparison with skeletal scintigraphy and FDG PET. Am J Roentgenol. 2001;177(1):229–36.
60. Byun BH, Kong C-B, Lim I, Kim BI, Choi CW, Song WS, et al. Comparison of (18)F-FDG PET/CT and (99 m)Tc-MDP bone scintigraphy for detection of bone metastasis in osteosarcoma. Skelet Radiol. 2013;42(12):1673–81.
61. Hurley C, McCarville MB, Shulkin BL, Mao S, Wu J, Navid F, et al. Comparison of ^{18} F-FDG-PET-CT and bone scintigraphy for evaluation of osseous metastases in newly diagnosed and recurrent osteosarcoma: ^{18} F-FDG-PET-CT for staging osteosarcoma. Pediatr Blood Cancer. 2016;63(8):1381–6.
62. Smets AM, Deurloo EE, Slager TJE, Stoker J, Bipat S. Whole-body magnetic resonance imaging for detection of skeletal metastases in children and young people with primary solid tumors—systematic review. Pediatr Radiol. 2018;48(2):241–52.
63. Paruthikunnan SM, Kadavigere R, Karegowda LH. Accuracy of whole-body DWI for metastases screening in a diverse group of malignancies: comparison with conventional cross-sectional imaging and nuclear scintigraphy. Am J Roentgenol. 2017;209(3):477–90.
64. Jacobs MA, Macura KJ, Zaheer A, Antonarakis ES, Stearns V, Wolff AC, et al. Multiparametric whole-body MRI with diffusion-weighted imaging and ADC mapping for the identification of visceral and osseous metastases from solid tumors. Acad Radiol [Internet]. 2018 [cited 2018 Jun 27]; Available from: http://linkinghub.elsevier.com/retrieve/pii/S1076633218300953

65. Saifuddin A, Mitchell R, Burnett SJ, Sandison A, Pringle JA. Ultrasound-guided needle biopsy of primary bone tumours. J Bone Joint Surg (Br). 2000;82(1):50–4.
66. Taupin T, Decouvelaere A-V, Vaz G, Thiesse P. Accuracy of core needle biopsy for the diagnosis of osteosarcoma: a retrospective analysis of 73patients. Diagn Interv Imaging. 2016;97(3):327–31.
67. Interiano RB, Malkan AD, Loh AHP, Hinkle N, Wahid FN, Bahrami A, et al. Initial diagnostic management of pediatric bone tumors. J Pediatr Surg. 2016;51(6):981–5.
68. Khoo MMY, Saifuddin A. The role of MRI in image-guided needle biopsy of focal bone and soft tissue neoplasms. Skelet Radiol. 2013;42(7):905–15.
69. Ahrar JU, Stafford RJ, Alzubaidi S, Ahrar K. Magnetic resonance imaging-guided biopsy in the musculoskeletal system using a cylindrical 1.5-T magnetic resonance imaging unit. Top Magn Reson Imaging. 2011;22(4):189–96.
70. Wu H-TH, Chang C-Y, Chang H, Yen C-C, Cheng H, Chen PC-S, et al. Magnetic resonance imaging guided biopsy of musculoskeletal lesions. J Chin Med Assoc. 2012;75(4):160–6.
71. Jeys LM, Thorne CJ, Parry M, Gaston CLL, Sumathi VP, Grimer JR. A novel system for the surgical staging of primary high-grade osteosarcoma: The Birmingham Classification. Clin Orthop Relat Res. 2017;475(3):842–50.
72. Cates JMM. Simple staging system for osteosarcoma performs equivalently to the AJCC and MSTS systems: OSTEOSARCOMA STAGING. J Orthop Res [Internet]. 2018 [cited 2018 Jun 27]; Available from: http://doi.wiley.com/10.1002/jor.24032
73. Jeon D-G, Cho WH, Song WS, Kong C-B, Cho SH, Lee JW, et al. Correlation between fluid–fluid levels on initial MRI and the response to chemotherapy in stage IIB osteosarcoma. Ann Surg Oncol. 2014;21(6):1956–62.
74. Jeon D-G, Song WS, Cho WH, Kong C-B, Cho SH. Proximal tumor location and fluid-fluid levels on MRI predict resistance to chemotherapy in stage IIB osteosarcoma. Clin Orthop Relat Res. 2014;472(6):1911–20.
75. Kim MS, Lee S-Y, Cho WH, Song WS, Koh J-S, Lee JA, et al. Growth patterns of osteosarcoma predict patient survival. Arch Orthop Trauma Surg. 2009;129(9):1189–96.
76. Lee JA, Kim MS, Kim DH, Lim JS, Yoo JY, Koh JS, et al. Relative tumor burden predicts metastasis-free survival in pediatric osteosarcoma. Pediatr Blood Cancer. 2008;50(2):195–200.
77. Kim SH, Shin K-H, Park EH, Cho YJ, Park B-K, Suh J-S, et al. A new relative tumor sizing method in epi-metaphyseal osteosarcoma. BMC Cancer. 2015 [cited 2018 Jun 27];15(1). Available from: http://bmccancer.biomedcentral.com/articles/10.1186/s12885-015-1129-9
78. Holscher HC, Bloem JL, Nooy MA, Taminiau AH, Eulderink F, Hermans J. The value of MR imaging in monitoring the effect of chemotherapy on bone sarcomas. AJR Am J Roentgenol. 1990;154(4):763–9.
79. Holscher HC, Bloem JL, Vanel D, Hermans J, Nooy MA, Taminiau AH, et al. Osteosarcoma: chemotherapy-induced changes at MR imaging. Radiology. 1992;182(3):839–44.
80. Holscher HC, Bloem JL, van der Woude HJ, Hermans J, Nooy MA, Taminiau AH, et al. Can MRI predict the histopathological response in patients with osteosarcoma after the first cycle of chemotherapy? Clin Radiol. 1995;50(6):384–90.
81. Shin KH, Moon SH, Suh JS, Yang WI. Tumor volume change as a predictor of chemotherapeutic response in osteosarcoma. Clin Orthop. 2000;376:200–8.
82. Amit P, Malhotra A, Kumar R, Kumar L, Patro D, Elangovan S. Evaluation of static and dynamic MRI for assessing response of bone sarcomas to preoperative chemotherapy: Correlation with histological necrosis. Indian J Radiol Imaging. 2015;25(3):269.
83. Laux CJ, Berzaczy G, Weber M, Lang S, Dominkus M, Windhager R, et al. Tumour response of osteosarcoma to neoadjuvant chemotherapy evaluated by magnetic resonance imaging as prognostic factor for outcome. Int Orthop. 2015;39(1):97–104.
84. Hanna SL, Parham DM, Fairclough DL, Meyer WH, Le AH, Fletcher BD. Assessment of osteosarcoma response to preoperative chemotherapy using dynamic FLASH gadolinium-DTPA-enhanced magnetic resonance mapping. Investig Radiol. 1992;27(5):367–73.
85. Guo J, Reddick WE, Glass JO, Ji Q, Billups CA, Wu J, et al. Dynamic contrast-enhanced magnetic resonance imaging as a prognostic factor in predicting event-free and overall survival in pediatric patients with osteosarcoma: DCE-MRI prognostic in osteosarcoma. Cancer. 2012;118(15):3776–85.
86. Bonnerot V, Charpentier A, Frouin F, Kalifa C, Vanel D, Di Paola R. Factor analysis of dynamic magnetic resonance imaging in predicting the response of osteosarcoma to chemotherapy. Investig Radiol. 1992;27(10):847–55.
87. Wakabayashi H, Saito J, Taki J, Hashimoto N, Tsuchiya H, Gabata T, et al. Triple-phase contrast-enhanced MRI for the prediction of preoperative chemotherapeutic effect in patients with osteosarcoma: comparison with 99mTc-MIBI scintigraphy. Skelet Radiol. 2016;45(1):87–95.
88. Kubo T, Furuta T, Johan MP, Adachi N, Ochi M. Percent slope analysis of dynamic magnetic resonance imaging for assessment of chemotherapy response of osteosarcoma or Ewing sarcoma: systematic review and meta-analysis. Skelet Radiol. 2016;45(9):1235–42.
89. Subhawong TK, Jacobs MA, Fayad LM. Insights into quantitative diffusion-weighted MRI for musculoskeletal tumor imaging. Am J Roentgenol. 2014;203(3):560–72.
90. Uhl M, Saueressig U, Koehler G, Kontny U, Niemeyer C, Reichardt W, et al. Evaluation of tumour necrosis during chemotherapy with diffusion-weighted MR imaging: preliminary results in osteosarcomas. Pediatr Radiol. 2006;36(12):1306–11.
91. Uhl M, Saueressig U, van Buiren M, Kontny U, Niemeyer C, Köhler G, et al. Osteosarcoma: preliminary results of in vivo assessment of tumor necrosis after chemotherapy with diffusion- and perfusion-weighted magnetic resonance imaging. Investig Radiol. 2006;41(8):618–23.
92. Oka K, Yakushiji T, Sato H, Hirai T, Yamashita Y, Mizuta H. The value of diffusion-weighted imaging for monitoring the chemotherapeutic response of osteosarcoma: a comparison between average apparent diffusion coefficient and minimum apparent diffusion coefficient. Skelet Radiol. 2010;39(2):141–6.
93. Wang C-S, Du L-J, Si M-J, Yin Q-H, Chen L, Shu M, et al. Noninvasive assessment of response to neoadjuvant chemotherapy in osteosarcoma of long bones with diffusion-weighted imaging: an initial in vivo study. Loeb D, editor. PLoS One. 2013;8(8):e72679.
94. Byun BH, Kong C-B, Lim I, Choi CW, Song WS, Cho WH, et al. Combination of 18F-FDG PET/CT and diffusion-weighted MR imaging as a predictor of histologic response to neoadjuvant chemotherapy: preliminary results in osteosarcoma. J Nucl Med. 2013;54(7):1053–9.
95. Wang J, Sun M, Liu D, Hu X, Pui MH, Meng Q, et al. Correlation between apparent diffusion coefficient and histopathology subtypes of osteosarcoma after neoadjuvant chemotherapy. Acta Radiol. 2017;58(8):971–6.
96. Baunin C, Schmidt G, Baumstarck K, Bouvier C, Gentet JC, Aschero A, et al. Value of diffusion-weighted images in differentiating mid-course responders to chemotherapy for osteosarcoma compared to the histological response: preliminary results. Skelet Radiol. 2012;41(9):1141–9.
97. Kubo T, Furuta T, Johan MP, Ochi M, Adachi N. Value of diffusion-weighted imaging for evaluating chemotherapy response in osteosarcoma: a meta-analysis. Mol Clin Oncol. 2017;7(1):88–92.

98. deSouza NM, Winfield JM, Waterton JC, Weller A, Papoutsaki M-V, Doran SJ, et al. Implementing diffusion-weighted MRI for body imaging in prospective multicentre trials: current considerations and future perspectives. Eur Radiol. 2018;28(3):1118–31.
99. Carrle D, Bielack SS. Current strategies of chemotherapy in osteosarcoma. Int Orthop. 2006;30(6):445–51.
100. Marina NM, Smeland S, Bielack SS, Bernstein M, Jovic G, Krailo MD, et al. Comparison of MAPIE versus MAP in patients with a poor response to preoperative chemotherapy for newly diagnosed high-grade osteosarcoma (EURAMOS-1): an open-label, international, randomised controlled trial. Lancet Oncol. 2016;17(10):1396–408.